

Adaptive Query Prompting for Multi-Domain Landmark Detection

Qiusen Wei¹, Guoheng Huang^{2*}, Xiaochen Yuan³, Xuhang Chen⁴, Guo Zhong⁵, Jianwen Huang², and Jiajie Huang²

¹School of Automation, Guangdong University of Technology, Guangzhou, China

²School of Computer Science and Technology, Guangdong University of Technology, Guangzhou, China

³Faculty of Applied Sciences, Macao Polytechnic University, Macao, China

⁴School of Computer Science and Engineering, Huizhou University, Huizhou, China

⁵School of Information Science and Technology, Guangdong University of Foreign Studies, Guangzhou, China

Abstract—Medical landmark detection is crucial in various medical imaging modalities and procedures. Although deep learning-based methods have achieved promising performance, they are mostly designed for specific anatomical regions or tasks. In this work, we propose a universal model for multi-domain landmark detection by leveraging transformer architecture and developing a prompting component, named as Adaptive Query Prompting (AQP). Instead of embedding additional modules in the backbone network, we design a separate module to generate prompts that can be effectively extended to any other transformer network. In our proposed AQP, prompts are learnable parameters maintained in a memory space called prompt pool. The central idea is to keep the backbone frozen and then optimize prompts to instruct the model inference process. Furthermore, we employ a lightweight decoder to decode landmarks from the extracted features, namely Light-MLD. Thanks to the lightweight nature of the decoder and AQP, we can handle multiple datasets by sharing the backbone encoder and then only perform partial parameter tuning without incurring much additional cost. It has the potential to be extended to more landmark detection tasks. We conduct experiments on three widely used X-ray datasets for different medical landmark detection tasks. Our proposed Light-MLD coupled with AQP achieves SOTA performance on many metrics even without the use of elaborate structural designs or complex frameworks.

I. INTRODUCTION

Landmark detection plays an important role in various of medical image analysis tasks [1], [2], [3]. It aims to localize anatomical keypoints in medical images such as X-ray images. Manual annotation is highly time-consuming, labor-intensive and typically requires a high level of expertise. Automatic annotation methods can significantly reduce the required labor and enable the analysis of large-scale datasets [4]. Despite the fact that deep learning-based methods have shown great promise on in the field of medical landmark detection, a significant limitation of many existing models is

* Corresponding author.

This work was supported in part by the Key Areas Research and Development Program of Guangzhou under Grant 2023B01J0029, Science and technology research in key areas in Foshan under Grant 2020001006832, the Science and technology projects of Guangzhou under Grant 202007040006, the Guangdong Provincial Key Laboratory of Cyber-Physical System under Grant 2020B1212060069, the Guangdong Basic and Applied Basic Research Foundation under Grant 2023A1515012534, and the National Statistical Science Research Project of China under Grant 2022LY096.

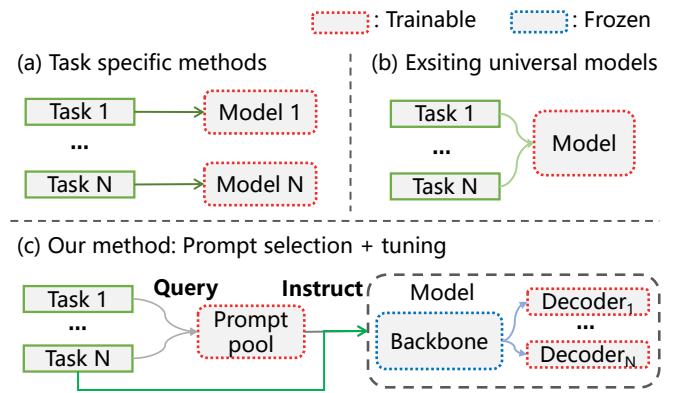


Fig. 1. Overview of the AQP framework. Compared with typical task-specific methods and existing universal models, which adapt entire model weights to deal with new tasks, AQP uses a single frozen backbone model and learns a prompt pool to instruct the model conditionally.

their task-specific nature. These models are typically tailored and refined to optimize performance within the confines of their designated tasks. Zhu et al. propose GU2Net [5] and DATR [6] as universal models for multi-domain landmark detection. However, these methods focus on elaborate structural designs to obtain better model performance, and require to train the entire model when handling new tasks, which is highly inefficient.

To this end, we propose *Adaptive Query Prompting* (AQP), a novel prompting method for multi-domain learning. Figure 1 gives an overview of our method in contrast to typical task specific methods and existing universal models. The basic idea is to efficiently adapt a frozen large foundation model to many downstream tasks with the minimum extra trainable parameters [7]. We keep the pre-trained model untouched, and instead learn a set of prompts that dynamically instruct model to solve corresponding tasks, it leverages the representative features from pre-trained models. The prompts are selected via a query-based mechanism. Specifically, prompts and keys are paired in a shared memory space called prompt pool, then we design a query function to get proper prompts paired with the keys, which are selected based on the query function. Our proposed AQP can select the appropriate prompt for various input, and does not require

complex design. The prompt pool, optimized jointly with the supervised loss, serves to ensure that shared prompts encode shared knowledge for effective knowledge transfer, while unshared prompts encode task-specific knowledge crucial for preserving model plasticity. The trainable parameters of our method is much fewer, thus being able to adapt to different tasks more efficiently.

In order to handle multiple landmark detection datasets without much extra cost, we employ a plain vision transformer as backbone to encode features and then adopt multiple lightweight decoders to deal with different tasks [8], [9], [10], [11]. For each iteration, we randomly sample instances from multiple training datasets and feed them into the backbone and the decoders to estimate the heatmaps corresponding to each dataset. Compared to previous methods, AQP enjoys the structure simplicity and can adapt well to different tasks through fine-tuning.

In summary, our main contributions can be outlined as follows:

- 1) We propose *Adaptive Query Prompting* (AQP), a novel prompt tuning method for multi-domain learning. It leads to better model generalization on the downstream tasks. We conduct the ablation to show the effectiveness of the prompting components.
- 2) We propose a unified transformer network for multi-domain landmark detection, namely Light-MLD, following the encoder-decoder pipeline. With the lightweight decoder, we can handle new tasks without incurring much additional cost.
- 3) In terms of experiments, we validate our method on three datasets for different medical landmark detection tasks: head, hand and chest. Our propose AQP achieves competitive performance with the whole model training and task-specific solutions without modification. Our model is simple but even outperforms previous state-of-the-art methods on many metrics.

II. RELATED WORK

A. Vision Transformer for Medical Landmark Detection

Recently, vision transformers [12], [13] have shown great potential in many vision tasks [14], [15], [16]. For instance, Xiao et al. [17] propose a lightweight Transformer-embedded network for vertebrae landmark detection, which has yielded promising results in this task. PRTR [18] incorporates both transformer encoders and decoders to gradually refine the locations of the estimated keypoints in a cascade manner. However, Most of these approaches employ a convolutional neural network (CNN) as a backbone, followed by the integration of a transformer with intricate architectures to enhance the extracted features and capture the relationships among the keypoints. They either necessitate CNNs for feature extraction or demand meticulous design of transformer architectures. In the contrast, ViTPose [13] employs a plain vision transformer [12] as the backbone with a simple decoder and obtains SOTA performance on representative benchmarks without elaborate designs. Follow its success, we introduced this framework into medical landmark detection.

B. Prompt Tuning

Prompting was originally introduced in the field of natural language processing (NLP) [19]. Shyam et al. [20] illustrates robust generalization to downstream transfer learning tasks, even in few-shot or zero-shot settings, utilizing manually selected prompts within GPT-3. Recently, the concept of prompting [21], [22] has been extended to vision tasks. Sandler et al. [22] introduces memory tokens, which are sets of trainable embedding vectors for each transformer layer. These traditional prompt tuning methods design task-specific prompt functions to instruct pre-trained models perform corresponding tasks conditionally [19], [23], so that the language model gets additional information about the task. However, crafting an effective prompting function poses a challenge, which require heuristic strategies. In this work, instead of designing a prompting function, we learn a set of prompts stored in the prompt pool. A query function is used to dynamically select suitable prompts tailored to different inputs. All that remains is the design of an effective query function, which is much easier than design prompts for different tasks. We can utilize the entire pre-trained model as a frozen feature extractor to obtain the query features.

III. METHOD

Problem Definition: Let D_1, D_2, \dots, D_N denote a set of N datasets, potentially originating from distinct anatomical regions. Given an image $I_i \in \mathbb{R}^{C_i \times H_i \times W_i}$ from Dataset D_i , along with corresponding landmarks $(x_{iC'_i}, y_{iC'_i})$, the k^{th} ($k \in [1, 2, \dots, C'_i]$) landmark's heatmap $Y_{ik} \in \mathbb{R}^{C'_i \times H_i \times W_i}$ is obtained using the Gaussian function:

$$Y_{ik} = \frac{1}{\sqrt{2\pi}\sigma} \exp\left(-\frac{(x-x_{ik})^2 + (y-y_{ik})^2}{2\sigma^2}\right), \quad (1)$$

where C_i represents the number of channels in the input image; C'_i denotes the number of channels in the output heatmap, namely the number of landmarks. The goal is to learn the Gaussian distribution (the heatmaps) corresponding to the landmarks.

A. Preliminaries

1) *ViTPose*: ViTPose [13] is a transformer-based network for human pose estimation. Similar to traditional CNN backbone [24], ViTPose captures multi-scale features via several stages. Differently, each stage is built via the feature embedding layers and vision transformer blocks [12], [25]. ViTPose adopt plain vision transformer with masked image modeling pre-training backbones, then pre-training the backbones using MAE [26] on MS COCO [27] dataset and a combination of MS COCO and AI Challenger [28] respectively by random masking 75% patches from the images and reconstructing those masked patches. In this work, we use the pre-trained weights to initialize the backbone of our model.

2) *Lightweight decoder*: Unlike the existing methods which use elaborate designs to decode the heatmaps from extracted features, we avoid introducing fancy but complex modules to keep the structure as simple as possible. We

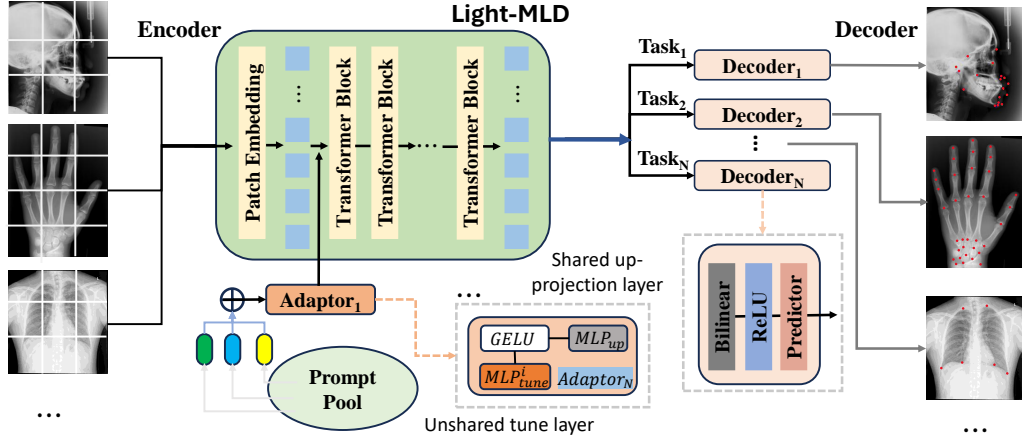


Fig. 2. The framework of Light-MLD. The backbone is consist of several feature embedding layers and vision transformer blocks, following by several decoder layers.

simply append several decoder layers after the transformer backbone to estimate the heatmaps. As shown in Figure 2, we directly utilize bilinear interpolation to upsample the feature maps by a factor of 4, followed by applying a Rectified Linear Unit (ReLU) and a convolutional layer with a kernel size of 3×3 to obtain the heatmaps, *i.e.*,

$$K = \text{Conv}_{3 \times 3}(\text{Bilinear}(\text{ReLU}(F_{out}))), \quad (2)$$

where F_{out} is the output feature of the transformer backbone. Since the simplicity and lightweight nature of the decoder, Light-MLD can effectively handle different tasks by incorporating multiple decoders without incurring much additional cost.

3) *Prompt-based learning*: Given an input of 2D image $I \in \mathbb{R}^{H \times W \times C}$ and a pre-trained vision transformer (ViT) backbone $f = f_r \circ f_e$ (excluding the decoder head), where f_r denotes transformer blocks [12], and f_e represents the patch embedding layer. Images are reshape to a sequence of flattened 2D patches $I^p \in \mathbb{R}^{N \times (C \cdot S)}$, where N is the number of patches. A image patch I^p is projected to a D -dimension feature through the patch embedding layer, *i.e.*, $f_e: \mathbb{R}^{N \times (C \cdot S)} \rightarrow \mathbb{R}^{S \times D}$, where D is the embedding dimension. The extracted features are denoted as x_e , and $x_e = f_e(I^p) \in \mathbb{R}^{S \times D}$. When employing prompt tuning methods, prompts can be fed into model in various ways. For example, a prompt $P_e \in \mathbb{R}^{L_p \times D}$ is considered as an additional token concatenated to the embedding feature x_e , where L_p is the token length. In a remarkable work called Explicit Visual Prompting (EVP) [7], prompts are first adjusted by a tunable adaptor, then added to the extracted embedding feature x_e through element-wise addition. This kind of prompt tuning typically yields better results because it learns explicit prompts. In this work, we adopt a approach similar to EVP.

B. Overview

As illustrated in Figure 2, Light-MLD employs a transformer-based backbone as encoder, which captures multi-stale features via several vision transformer blocks,

then followed by a series of lightweight decoders to decode the corresponding landmarks for different tasks. Figure 3 gives a overview our proposed *Adaptive Query Prompting* (AQP). Prompts are selected from the prompt pool to instruct the model during training process.

C. Adaptive query prompting

In our proposed adaptive query prompting, there are three main components, namely the Prompt pool, the Prompt query mechanism and the Adaptor.

1) *Prompt pool*: The reasons for adopting prompt pooling are twofold. On the one hand, designing an effective prompt generation function is nontrivial, especially for a generic landmark detection model. On the other hand, a shared prompt pool enables knowledge transfer between different tasks, since there are commonalities between different tasks. Thus, we employ a *prompt pool* to store encoded knowledge, which can be flexibly grouped as input to the model. The prompt pool is defined as

$$\mathbf{P} = \{P_1, P_2, \dots, P_N\}, \quad (3)$$

where N represents total number of prompts. $P_j \in \mathbb{R}^{L_p \times D}$ is a single prompt with the same embedding size D as x_e and token length L_p . x_e is extracted embedding feature projected by the embedding layer.

2) *Prompt query mechanism*: In order to efficiently select suitable prompts for different inputs, We propose an approach of query strategy based on key-value pairs, which dynamically determines appropriate prompts for varying inputs. As shown in Figure 3, this query mechanism relies on key-valued memory, which uses external memory for distinct computational objectives. Each prompt is associated with a learnable key in the form of $(k_1, P_1), (k_2, P_2), \dots, (k_N, P_N)$, where $k_i \in \mathbb{R}^{D_k}$. The collection of all keys is denoted as $\mathbf{K} = \{k_i\}_{i=1}^N$. Ideally, we aim to enable the input instance itself to determine the prompts to select via query-key matching. For this purpose, we introduce a query function $q: \mathbb{R}^{H \times W \times C} \rightarrow \mathbb{R}^{D_k}$ that encodes the input I to the same

dimension as the keys in the prompt pool. Furthermore, q should be a deterministic function across different tasks and devoid of learnable parameters. In this work, we utilize the pre-trained transformer backbone as a fixed feature extractor to obtain the query features.

Let $\gamma: \mathbb{R}^{D_k} \times \mathbb{R}^{D_k} \rightarrow \mathbb{R}$ represent a function that scores the match between the query and prompt key (in this work we adopt cosine distance). When presented with an input x , we use $q(x)$ to retrieve the top- M keys by straightforwardly solving the objective function:

$$\mathbf{K}_x = \underset{\{s_i\}_{i=1}^M \subseteq [1, N]}{\operatorname{argmin}} \sum_{i=1}^M \gamma(q(x), \mathbf{k}_{s_i}), \quad (4)$$

where \mathbf{K}_x denotes a subset of top- M keys specifically chosen for x from \mathbf{K} . Furthermore, the querying of prompts is performed on an instance-wise basis, rendering the entire framework task-agnostic, which enhances its generality.

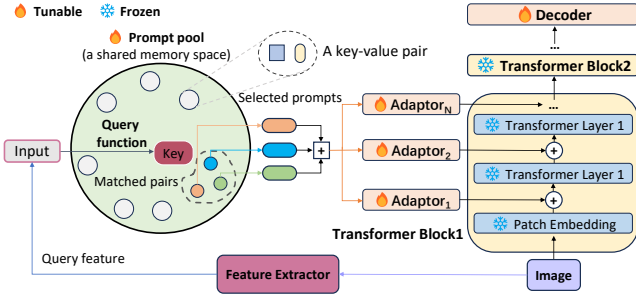


Fig. 3. The architecture of the proposed AQP, where the operator \boxplus denotes concatenate and \oplus means element-wise addition. The goal of the Adaptor is to merge selected prompts and align them with the input.

3) *Adaptor*: The objective of the Adaptor is to conduct adaptation efficiently and effectively across all layers, incorporating features from all the prompts selected from the prompt pool. Denote P as the concatenation of M selected prompts, $P = [P_1, P_2, \dots, P_M]$. For the i -th Adaptor, we take P as input to generate the final prompting P_f^i :

$$P_f^i = MLP_{up}(GELU(MLP_{tune}^i(P))), \quad (5)$$

where MLP_{up} represents an up-projection layer shared across all Adaptors, aimed at aligning the dimensions of transformer feature. $GELU$ denotes the GELU activation function [29]. MLP_{tune} is a linear layer responsible for generating distinct prompts in each Adaptor. P_f^i is the output prompt that attaches to each transformer layer. This design allows for strong adaptability while generating diverse prompts. With the adaptor, we can generate suitable prompts for all tasks in a unified paradigm even when using different models or backbones.

D. Training

1) *Prompting details*: Here we elaborate on some details about prompting during training process. Given an image input x , we first obtain the query features through a feature extractor. In this work, we directly adopt the entire pre-trained model as a frozen feature extractor, other pre-trained

model like ConvNet are feasible as well. The corresponding query features is denoted as $q(x)$. After obtaining the query features, we derive the corresponding keys by simply solving Equation 4, where γ is a function used to measure the degree of matching between query features and keys, namely the query function. M is a hyperparameter determines the number of prompts selected in the prompt pool. Here we use cosine similarity as the measure. The selected prompts are concatenated then fed into the adaptors, which perform adaptation across all the layers, as shown in Figure 3. Finally, the output prompts are attached to each transformer layer guiding the model’s inference process.

2) *Loss function*: In this work, we jointly train the two components, the original model and the prompt pool. Overall, we seek to minimize the following training loss function:

$$\mathcal{L} = \frac{1}{2N} \sum_{j=0}^{N-1} \|H^j - G^j\|_2 + \lambda \sum_{\mathbf{K}_x} \gamma(q(x), \mathbf{k}_{s_i}), \quad (6)$$

where \mathbf{K}_x is obtained with Equation (4).

The first term is the heatmap MSE loss \mathcal{L}_{ht} , where H^j represents the predicted heatmap for the j -th keypoint, G^j denotes the corresponding ground truth gaussian heatmap for the j -th keypoint. N is the total number of keypoints, and $\|\cdot\|_2$ denotes the L2 norm between the predicted and ground truth heatmaps. The second term serves as a surrogate loss to bring the selected keys closer to their corresponding query features, and λ is a scalar used to weight the loss.

IV. EXPERIMENTS

In this section, we conduct quantitative and qualitative evaluations of our universal model, comparing it with SOTA methods on three public X-ray datasets of head, hand and chest for different medical landmark detection tasks. Moreover, we conduct extensive ablation studies to demonstrate the effectiveness of the proposed AQP.

A. Datasets

1) *Head*: The head dataset is a widely-used public dataset for cephalometric landmark detection, which contains 400 X-ray images, provided in IEEE ISBI 2015 challenge [30]. It contains 19 landmarks for each X-ray image. For our experimentation, we designate the first 150 images for training and the remaining 250 images for testing purposes.

2) *Hand*: The hand dataset comprises 909 X-ray images. We allocate the first 609 images for training and reserve the remaining 300 images for testing. Payer et al. [31] manually labeled a total of 37 landmarks.

3) *Chest*: The chest dataset comprises 279 X-ray images. The initial 229 images are allocated for training, and the remaining 50 images are reserved for testing purposes. There are six landmarks labeled in each chest X-ray image, which delineate the boundary of the lung.

B. Settings

For model training, we adopt the AdamW optimizer with an initial learning rate of $5e^{-4}$. Cosine decay is employed

TABLE I

QUALITY METRICS OF DIFFERENT MODELS ON HEAD AND HAND DATASETS. + REPRESENTS THE MODEL IS LEARNED ON THE MIXED DATASETS. THE BEST RESULTS ARE IN **BOLD** AND THE SECOND BEST RESULTS ARE UNDERLINED.

Models	MRE (mm)	Head SDR(%)				MRE (mm)	Hand SDR(%)			MRE (px)	Chest SDR(%)		
		2mm	2.5mm	3mm	4mm		2mm	4mm	10mm		3px	6px	9px
Ibragimov et al. [32]	1.84	68.13	74.63	79.77	86.87	-	-	-	-	-	-	-	
Štern et al. [33]	-	-	-	-	-	0.80	92.20	98.45	99.83	-	-	-	
Lindner et al. [34]	1.67	70.65	76.93	82.17	89.85	0.85	93.68	98.95	99.94	-	-	-	
Urschler et al. [35]	-	70.21	76.95	82.08	89.01	0.80	92.19	98.46	99.95	-	-	-	
Payer et al. [36]	-	73.33	78.76	83.24	89.75	0.66	94.99	99.27	99.99	-	-	-	
U-Net [37]+	12.45	52.08	60.04	66.54	73.68	6.14	81.16	92.46	93.76	5.64	51.67	82.33	
GU2Net [5]+	<u>1.56</u>	77.79	84.65	<u>89.41</u>	<u>94.93</u>	0.84	<u>95.40</u>	<u>99.35</u>	99.75	5.57	57.33	82.67	
AQP (Ours)+	1.54	<u>76.39</u>	<u>84.43</u>	89.61	95.02	<u>0.76</u>	96.27	99.45	<u>99.79</u>	<u>5.61</u>	<u>56.78</u>	83.46	

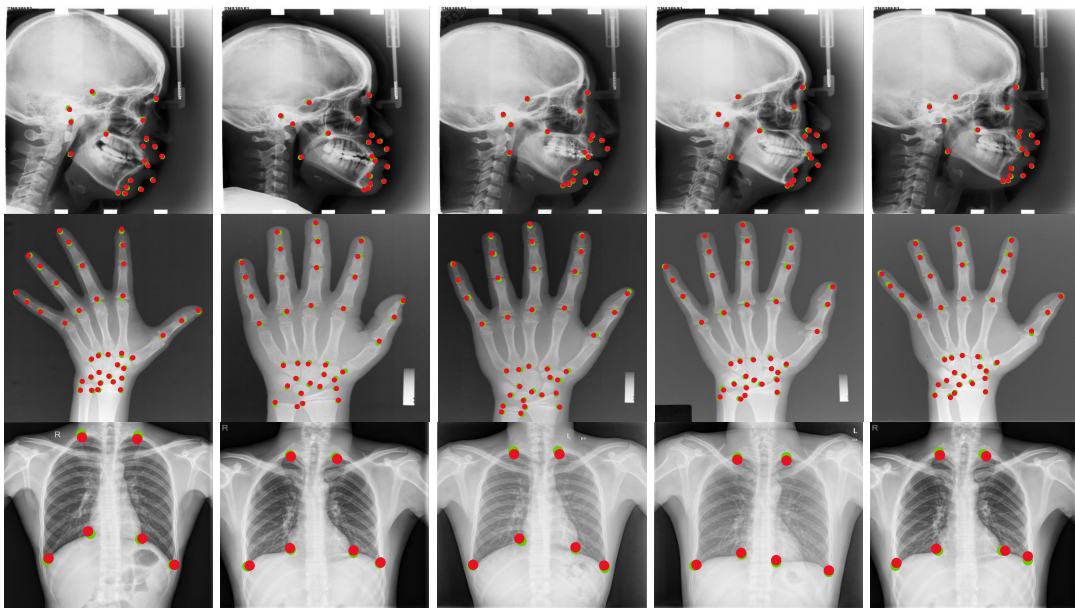


Fig. 4. Subjective results of the head and hand datasets. All images are randomly selected. The red points \bullet are the landmarks predicted by our model while the green points \bullet are the ground truth labels.

to adjust the learning rate over time. We use the ViTPose-L as backbones for test, which are pre-trained on MS COCO Keypoint Detection Dataset [27], corresponding to ViT-Large. The models are trained 25 epochs for all datasets. The images are resized to the shape of 256×192 for all datasets.

C. Evaluation and results

For the evaluation metric, we use the mean radial error (MRE) to measure the Euclidean distance between prediction and ground truth, and the successful detection rate (SDR).

Table I presents the experimental results on the the head, hand and chest datasets. Here we adopt the ViTPose-L as backbone and fine-tune the model with AQP on these datasets. From the experimental results, it can be observed that our Light-MLD with AQP achieves performance comparable to the previous SOTA methods. On the head dataset, Light-MLD achieved the best accuracy of 89.61% within 3mm and 95.62% within 4mm, and second-best performance on the remaining metrics, falling just slightly behind the best-performing model. On the hand dataset, Light-MLD outperforms the previous SOTA method for SDR within 2mm

and 3mm. On the chest dataset, our model also reaches the best accuracy of 83.46% with 6px, but a little worse on the other metrics. Overall, our model achieve the best or second-best performance on the three datasets across all metrics, and performs better than models that are learned on a single dataset. We also provide some visual landmark detection results for subjective evaluation, as shown in Figure 4. We demonstrate the results on head, hand and chest datasets respectively.

D. Ablation Study

We conduct the ablation study to demonstrate the effectiveness of our proposed AQP. Moreover, we compared the results using different vision transformer backbones on the head dataset. Here, we employed three different backbones for testing, namely ViTPose-S, ViTPose-B and ViTPose-L. From the experimental results in Table II, it can be observed that after training with AQP, the model exhibits significant improvements across multiple metrics. Introducing additional prompts effectively increases the trainable parameters, thus enhancing the model’s representational capacity.

TABLE II

ABLATION STUDY OF OUR UNIVERSAL MODEL WITH PROMPT TUNING METHOD USING DIFFERENT BACKBONES. # DENOTES THE MODELS ARE FINE-TUNED WITH AQP.

Model	MRE(↓)		SDR(↑)(%)		
	mm	2mm	2.5mm	3mm	4mm
ViTPose-S	1.83	67.31	74.36	79.71	86.52
ViTPose-S#	1.73	69.89	77.03	82.01	89.55
ViTPose-B	1.76	70.24	76.59	82.17	89.77
ViTPose-B#	1.63	74.89	80.23	86.91	92.03
ViTPose-L	1.62	75.81	80.71	86.54	92.68
ViTPose-L#	1.56	76.39	83.43	89.61	95.02

V. CONCLUSIONS

This paper presents Adaptive Query Prompting (AQP) for Multi-Domain Landmark Detection. Our universal model Light-MLD is simple yet powerful, consisting only of a plain vision transformer backbone and a simple decoder. Furthermore, the proposed AQP can effectively instruct the model perform better without incurring much additional cost. Experimental results demonstrate that our proposed method performs well in different landmark detection tasks, even outperforms previous state-of-the-art methods on many metrics. For future work, we will derive more complex framework to test the effectiveness of our AQP, since the model in this work is quite simple.

REFERENCES

- [1] X. Chen, B. Lei, C.-M. Pun, and S. Wang, "Brain diffuser: An end-to-end brain image to brain network pipeline," in *PRCV*, 2023, pp. 16–26.
- [2] C. Gong, C. Jing, X. Chen, C.-M. Pun, G. Huang, A. Saha, M. Nieuwoudt, H.-X. Li, Y. Hu, and S. Wang, "Generative ai for brain image computing and brain network computing: a review," *Frontiers in Neuroscience*, vol. 17, 2023.
- [3] G. Huang, X. Chen, Y. Shen, and S. Wang, "Mr image super-resolution using wavelet diffusion for predicting alzheimer's disease," in *BI*, 2023.
- [4] J. Ma, Y. He, F. Li, L. Han, C. You, and B. Wang, "Segment anything in medical images," *Nature Communications*, vol. 15, no. 1, p. 654, 2024.
- [5] H. Zhu, Q. Yao, L. Xiao, and S. K. Zhou, "You only learn once: Universal anatomical landmark detection," in *MICCAI*. Springer, 2021, pp. 85–95.
- [6] H. Zhu, Q. Yao, and S. K. Zhou, "Datr: domain-adaptive transformer for multi-domain landmark detection," *arXiv*, 2022.
- [7] W. Liu, X. Shen, C.-M. Pun, and X. Cun, "Explicit visual prompting for low-level structure segmentations," in *CVPR*, 2023, pp. 19434–19445.
- [8] Z. Li, X. Chen, S. Wang, and C.-M. Pun, "A large-scale film style dataset for learning multi-frequency driven film enhancement," in *IJCAI*, 2023, pp. 1160–1168.
- [9] Z. Li, X. Chen, C.-M. Pun, and X. Cun, "High-resolution document shadow removal via a large-scale real-world dataset and a frequency-aware shadow erasing net," *ICCV*, pp. 12415–12424, 2023.
- [10] S. Luo, X. Chen, W. Chen, Z. Li, S. Wang, and C.-M. Pun, "Devignet: High-resolution vignetting removal via a dual aggregated fusion transformer with adaptive channel expansion," in *AAAI*, 2023.
- [11] W. Liu, X. Cun, C.-M. Pun, M. Xia, Y. Zhang, and J. Wang, "Coordfill: Efficient high-resolution image inpainting via parameterized coordinate querying," in *AAAI*, 2023.
- [12] A. Dosovitskiy, L. Beyer, A. Kolesnikov, D. Weissenborn, X. Zhai, T. Unterthiner, M. Dehghani, M. Minderer, G. Heigold, S. Gelly *et al.*, "An image is worth 16x16 words: Transformers for image recognition at scale," *arXiv*, 2020.
- [13] Y. Xu, J. Zhang, Q. Zhang, and D. Tao, "Vitpose: Simple vision transformer baselines for human pose estimation," *NIPS*, vol. 35, pp. 38571–38584, 2022.
- [14] X. Chen, X. Cun, C.-M. Pun, and S. Wang, "Shadocnet: Learning spatial-aware tokens in transformer for document shadow removal," *ICASSP*, pp. 1–5, 2022.
- [15] Z. Li, X. Chen, C.-M. Pun, and S. Wang, "Wavenhancer: Unifying wavelet and transformer for image enhancement," *arXiv*, 2022.
- [16] W. Liu, X. Shen, H. Li, X. Bi, B. Liu, C.-M. Pun, and X. Cun, "Depth-aware test-time training for zero-shot video object segmentation," *arXiv*, 2024.
- [17] Q. Xiao, Y. Chen, J. Wang, F. Zang, Y. Wang, G. Zheng, K. Yang, R. Zhang, B. Hu, and H. Chen, "Application of tvd-net for sagittal alignment and instability measurements in cervical spine radiographs," *Medical Physics*, 2023.
- [18] K. Li, S. Wang, X. Zhang, Y. Xu, W. Xu, and Z. Tu, "Pose recognition with cascade transformers," in *CVPR*, 2021, pp. 1944–1953.
- [19] P. Liu, W. Yuan, J. Fu, Z. Jiang, H. Hayashi, and G. Neubig, "Pre-train, prompt, and predict: A systematic survey of prompting methods in natural language processing," *ACM Computing Surveys*, vol. 55, no. 9, pp. 1–35, 2023.
- [20] T. Brown, B. Mann, N. Ryder, M. Subbiah, J. D. Kaplan, P. Dhariwal, A. Neelakantan, P. Shyam, G. Sastry, A. Askell *et al.*, "Language models are few-shot learners," *NIPS*, vol. 33, pp. 1877–1901, 2020.
- [21] M. Jia, L. Tang, B.-C. Chen, C. Cardie, S. Belongie, B. Hariharan, and S.-N. Lim, "Visual prompt tuning," in *ECCV*. Springer, 2022, pp. 709–727.
- [22] M. Sandler, A. Zhmoginov, M. Vladymyrov, and A. Jackson, "Fine-tuning image transformers using learnable memory," in *CVPR*, 2022, pp. 12155–12164.
- [23] X. Chen, C.-M. Pun, and S. Wang, "Medprompt: Cross-modal prompting for multi-task medical image translation," *ArXiv*, 2023.
- [24] K. He, X. Zhang, S. Ren, and J. Sun, "Deep residual learning for image recognition," in *CVPR*, 2016, pp. 770–778.
- [25] A. Vaswani, N. Shazeer, N. Parmar, J. Uszkoreit, L. Jones, A. N. Gomez, Ł. Kaiser, and I. Polosukhin, "Attention is all you need," *NIPS*, vol. 30, 2017.
- [26] K. He, X. Chen, S. Xie, Y. Li, P. Dollár, and R. Girshick, "Masked autoencoders are scalable vision learners," in *CVPR*, 2022, pp. 16000–16009.
- [27] T.-Y. Lin, M. Maire, S. Belongie, J. Hays, P. Perona, D. Ramanan, P. Dollár, and C. L. Zitnick, "Microsoft coco: Common objects in context," in *ECCV*. Springer, 2014, pp. 740–755.
- [28] J. Wu, H. Zheng, B. Zhao, Y. Li, B. Yan, R. Liang, W. Wang, S. Zhou, G. Lin, Y. Fu *et al.*, "Large-scale datasets for going deeper in image understanding," in *ICME*. IEEE, 2019, pp. 1480–1485.
- [29] D. Hendrycks and K. Gimpel, "Gaussian error linear units (gelus)," *arXiv*, 2016.
- [30] C.-W. Wang, C.-T. Huang, J.-H. Lee, C.-H. Li, S.-W. Chang, M.-J. Siao, T.-M. Lai, B. Ibragimov, T. Vrtovec, O. Ronneberger *et al.*, "A benchmark for comparison of dental radiography analysis algorithms," *Medical image analysis*, vol. 31, pp. 63–76, 2016.
- [31] C. Payer, D. Štern, H. Bischof, and M. Urschler, "Integrating spatial configuration into heatmap regression based cnns for landmark localization," *Medical image analysis*, vol. 54, pp. 207–219, 2019.
- [32] S. Ioffe and C. Szegedy, "Batch normalization: Accelerating deep network training by reducing internal covariate shift," in *ICML*. pmlr, 2015, pp. 448–456.
- [33] D. Štern, T. Ebner, and M. Urschler, "From local to global random regression forests: exploring anatomical landmark localization," in *MICCAI*. Springer, 2016, pp. 221–229.
- [34] C. Lindner, P. A. Bromiley, M. C. Ionita, and T. F. Cootes, "Robust and accurate shape model matching using random forest regression-voting," *IEEE transactions on pattern analysis and machine intelligence*, vol. 37, no. 9, pp. 1862–1874, 2014.
- [35] M. Urschler, T. Ebner, and D. Štern, "Integrating geometric configuration and appearance information into a unified framework for anatomical landmark localization," *Medical image analysis*, vol. 43, pp. 23–36, 2018.
- [36] C. Payer, D. Štern, H. Bischof, and M. Urschler, "Integrating spatial configuration into heatmap regression based cnns for landmark localization," *Medical image analysis*, vol. 54, pp. 207–219, 2019.
- [37] O. Ronneberger, P. Fischer, and T. Brox, "U-net: Convolutional networks for biomedical image segmentation," in *MICCAI*. Springer, 2015, pp. 234–241.